inorganics

MDPI

Article

Coordination Polymers Constructed from Polycarboxylic Acids and Semi-Rigid Bis-pyridyl-bis-imide Ligands: Synthesis, Structures and Iodine Adsorption

Yi-Wun Chen, Zhi-Ling Chen, Song-Wei Wang and Jhy-Der Chen *

Department of Chemistry, Chung Yuan Christian University, Chung Li, Taoyuan City 320, Taiwan; s10713146@gmail.com (Y.-W.C.); mandy093999@gmail.com (Z.-L.C.); bvbv20520@gmail.com (S.-W.W.)
* Correspondence: jdchen@cycu.edu.tw; Tel.: +886-3-265-3351

Abstract: Reactions of *N*,*N*′-bis(3-pyridylmethyl)-pyromellitic diimide (**L**^{1}) or *N*,*N*′-bis(3-pyridyl)bicyclo(2,2,2,)oct-7-ene-2,3,5,6-tetracarboxylic diimide (**L**^{2}) with 1,3,5-benzenetricarboxylic acid (1,3,5-H_3BTC), 4,4′-sulfonyldibenzoic acid (H_2SDA), or 4,4′-oxybisbenzoic acid (H_2OBA) and divalent metal salts afforded {[Co(1,3,5-HBTC)(H_2O)$_2$(**L**^{1})]·H_2O}$_n$, **1**, {[Co(1,3,5-HBTC)(H_2O)$_3$(**L**^{1})$_{0.5}$]·H_2O}$_n$, **2**, {[Co(SDA)(**L**^{1})$_{0.5}$]·H_2O}$_n$, **3**, {[Co(1,3,5-HBTC)(H_2O(**L**^{2}))]·H_2O}$_n$, **4**, {[Ni(1,3,5-HBTC)(H_2O)(**L**^{2})]·H_2O}$_n$, **5**, [Ni(SDA)(**L**^{2})]$_n$, **6**, and [Ni(OBA)(**L**^{2})]$_n$, **7**, which were structurally characterized by using single-crystal X-ray diffraction. Complexes **1** and **2** are 1D chains with the 2,4C6 and 2,3C2 topologies, respectively, and **3** is a 2D layer with the 4,5L51 topology, whereas **4** and **5** are 1D chains with the 2,4C6 topology and **6** and **7** are 2D layers with the 2,4L2 topology. Complex **3** shows a better iodine-adsorption factor of 133.77 mg g^{-1} at 75 °C for 24 h than **5**–**7**, revealing that the pi-pi conjugation of the dipyridyl ligand may govern the iodine adsorption capacity.

Keywords: coordination polymer; X-ray structure; topology; dipyridyl ligand; iodine adsorption

check for updates

Academic Editor: László Kótai

Received: 9 February 2025
Revised: 22 February 2025
Accepted: 24 February 2025
Published: 26 February 2025

Citation: Chen, Y.-W.; Chen, Z.-L.; Wang, S.-W.; Chen, J.-D. Coordination Polymers Constructed from Polycarboxylic Acids and Semi-Rigid Bis-pyridyl-bis-imide Ligands: Synthesis, Structures and Iodine Adsorption. *Inorganics* **2025**, *13*, 69. https://doi.org/10.3390/inorganics13030069

Copyright: © 2025 by the authors. Licensee MDPI, Basel, Switzerland. This article is an open access article distributed under the terms and conditions of the Creative Commons Attribution (CC BY) license (https://creativecommons.org/licenses/by/4.0/).

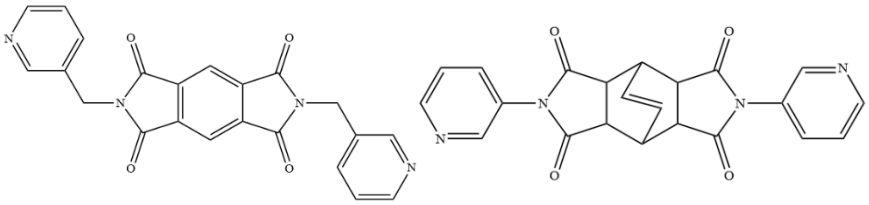
1. Introduction

Due to their designable structures and variable functions, coordination polymers (CPs) have shown potential applications in areas such as ion exchange, sensor, catalysis, gas storage, and magnetism [1–5]. Therefore, CPs have attracted widespread attention and research in the chemical community. However, designing and forming CPs with unique structures and functions remain challenges. The coordination of the spacer ligands to the metal ions may result in CPs with one-dimensional (1D), two-dimensional (2D), or three-dimensional (3D) structures, which are susceptible to changes in the metal ion, spacer ligand, solvent system, and reaction temperature. On the other hand, the separation and recovery of toxic radioactive iodine such as ^{129}I are essential for human health. CPs showing tailorable structures and possessing pores that may facilitate iodine adsorption through noncovalent interactions are thus demanded [6–22].

In the self-assembly processes of CPs, the identities of the spacer ligands involving the length, flexibility, and orientation of the donor atom may govern the structural diversity. By using the flexible ligands *N*,*N*′-di(4-pyridyl)sebacoamide or *N*,*N*′-di(4-pyridyl)adipoamide and angular dicarboxylate ligands, five entangled CPs, and one non-entangled CP, were obtained [23], whereas the use of the rigid *N*,*N*′-bis(4-pyridylmethyl)bicyclo(2,2,2,)oct-7-ene-2,3,5,6-tetracarboxylic diamide afforded three non-entangled CPs and one entangled

CP, respectively [23]. We thus proposed that Co(II) CPs containing flexible bis-pyridyl-bis-amide (bpba) and angular dicarboxylate ligands are more likely to form entangled networks than those with rigid ones [23].

To further investigate the role of rigid spacer ligands in determining the structural diversity of CPs supported by polycarboxylate ligands, *N*,*N*′-bis(3-pyridylmethyl)-pyromellitic diimide (**L**^{1}) [24–30], Figure 1a, and *N*,*N*′-bis(3-pyridyl)bicyclo(2,2,2,)oct-7-ene-2,3,5,6-tetracarboxylic diimide (**L**^{2}) [31,32], Figure 1b, were prepared to react with polycarboxylic acids and divalent salts to study the structural diversity of the CPs thus prepared. Herein, the synthesis and structures of {[Co(1,3,5-HBTC)(H_2O)$_2$(**L**^{1})]·H_2O}$_n$, **1**, {[Co(1,3,5-HBTC)(H_2O)$_3$(**L**^{1})$_{0.5}$]·H_2O}$_n$, **2**, {[Co(SDA)(**L**^{1})$_{0.5}$]·H_2O}$_n$, **3**, {[Co(1,3,5-HBTC)(H_2O(**L**^{2}))]·H_2O}$_n$, **4**, {[Ni(1,3,5-HBTC)(H_2O)(**L**^{2})]·H_2O}$_n$, **5**, [Ni(SDA)(**L**^{2})]$_n$, **6**, and [Ni(OBA)(**L**^{2})]$_n$, **7**, form the subject of this report. The iodine adsorption of complexes **3**, **5**, **6**, and **7** are also evaluated.



(**a**) (**b**)

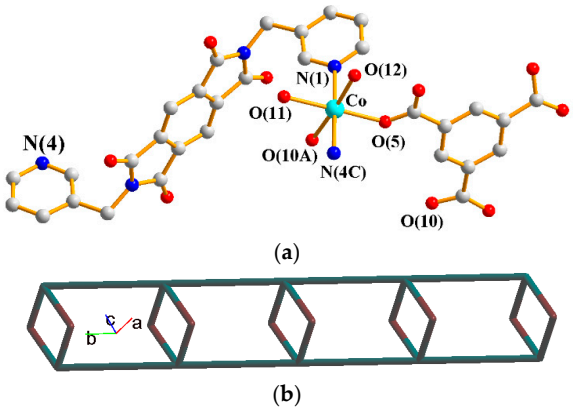
Figure 1. Structures of (**a**) **L**^{1}, (**b**) **L**^{2}.

2. Results and Discussion

The structures of complexes **1**, **3**, **4**, and **5** were solved in the triclinic space group *P*$\bar{1}$, and **2** in the monoclinic $P2_1/c$, respectively, whereas **6** and **7** were solved in the monoclinic $C2/c$.

2.1. Structure of **1**

The asymmetric unit consists of one Co(II) cation, one **L**^{1} ligand, one 1,3,5-HBTC^{2-} ligand, two coordinated water molecules and one crystallized water molecule. Figure 2a shows the coordination environment around the Co(II) metal center, which is six-coordinated by two nitrogen atoms from two **L**^{1} ligands [Co–N = 2.165(3)–2.193(3) Å], two oxygen atoms from two 1,3,5-HBTC^{2-} ligands [Co–O = 2.076(2)–2.095(3) Å], and two oxygen atoms from two coordination water molecules [Co–O = 2.096(3)–2.136(3) Å]. The Co(II) cations are linked by 1,3,5-HBTC^{2-} and **L**^{1} ligands to form 1D looped chains. If the Co(II) ions are defined as 4-connected nodes and 1,3,5-HBTC^{2-} ligands as 2-connected nodes, whereas the **L**^{1} ligands are defined as linkers, the structure can be simplified as a 2,4-connected 1D net with a {4.6^4.8}{4}-2,4C6 topology (Figure 2b), as determined using ToposPro [33].



(**a**)

(**b**)

Figure 2. (**a**) Coordination environment around the Co(II) ion of **1**. Symmetry transformations used to generate equivalent atoms: (A) −x + 1, −y + 1, −z + 1; (B) x, y − 1, z; (C) x, y + 1, z. (**b**) A drawing showing the 2,4C6 topology.

2.2. Structure of **2**

The asymmetric unit consists of one Co(II) cation, half of an $\mathbf{L^1}$ ligand, one 1,3,5-HBTC^{2-} ligand, three coordinated water molecules, and one crystallized water molecule. Figure 3a shows the coordination environment around the Co(II) metal center, which is six-coordinated by one nitrogen atom from the $\mathbf{L^1}$ ligand [Co–N = 2.1231(18) Å], two oxygen atoms from two 1,3,5-HBTC^{2-} ligands [Co–O = 2.0407(14)–2.0945(14) Å] and three oxygen atoms from three coordination water molecules [Co-O = 2.0945(15)–2.1803(16) Å]. The Co(II) cations are linked by 1,3,5-HBTC^{2-} and $\mathbf{L^1}$ ligands to form 1D looped chains. If the Co(II) units are defined as 3-connected nodes and 1,3,5-HBTC^{2-} ligands as 2-connected nodes, whereas the $\mathbf{L^1}$ ligands are defined as linkers, the structure of **2** can be simplified as a 2,3-connected 1D net with a {4}-2,3C2 topology, as shown in Figure 3b.

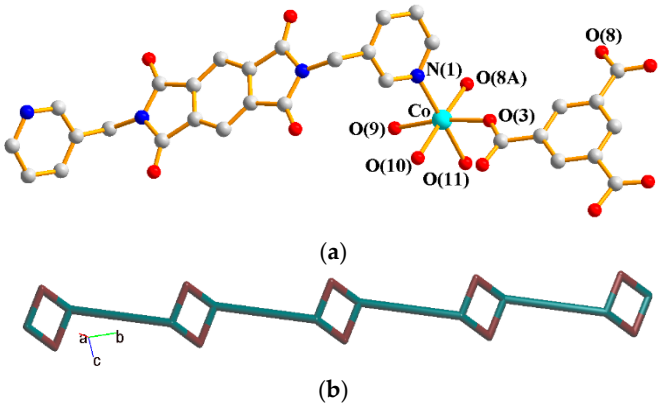


Figure 3. (**a**) Coordination environment around the Co(II) ion of **2**. Symmetry transformations used to generate equivalent atoms: (A) −x + 1, −y + 1, −z + 2; (B) −x, −y + 2, −z + 2. (**b**) A drawing showing the 2,3C2 topology.

It is interesting to note that the subtle difference in the structures between complexes **1** and **2**, 1D looped chains with {4.6^4.8}{4}-2,4C6 and {4}-2,3C2 topologies, respectively, can be ascribed to the different molar ratios of the reagents, Co(OAc)$_2$·4H$_2$O:$\mathbf{L^1}$:1,3,5-H$_3$BTC, for preparations of **1** and **2** that are 1:1:1 and 3:1:2, respectively.

2.3. Structure of **3**

The asymmetric unit consists of one Co(II) cation, half of an $\mathbf{L^1}$ ligand, one SDA^{2-} ligand, and one crystallized water molecule. Figure 4a shows the coordination environment around the Co(II) metal center, which is six-coordinated by one nitrogen atom from two $\mathbf{L^2}$ ligands [Co–N = 2.055(2) Å] and five oxygen atoms from two SDA^{2-} ligands [Co–O =2.0168(18)–2.3641(19) Å]. The Co(II) cations are linked by SDA^{2-} to form 2D layers. If the Co(II) ions are defined as 5-connected nodes and SDA^{2-} as 4-connected nodes, whereas the $\mathbf{L^2}$ ligands are defined as linkers, the structure of **3** can be simplified as a 4,5-connected 2D net with a {4^6·6^4}{4^6}-4,5L51 topology, Figure 4b.

2.4. Structure of **4**

The asymmetric unit consists of one Co(II) cation, one $\mathbf{L^2}$ ligand, one 1,3,5-HBTC^{2-} ligand, one coordinated water molecule, and one crystallized water molecule. Figure 5a shows the coordination environment around the Co(II) metal center, which is six-coordinated by two nitrogen atoms from two $\mathbf{L^2}$ ligands [Co–N = 2.147(4)–2.156(4) Å], three oxygen atoms from two 1,3,5-HBTC^{2-} ligands [Co–O = 2.043(3)–2.209(3) Å], and one oxygen atom from one coordination water molecule [Co–O = 2.065(3) Å]. The Co(II) cations are linked by 1,3,5-HBTC^{2-} and $\mathbf{L^2}$ ligands to form 1D chains. If the Co(II) units are defined as 4-connected nodes and $\mathbf{L^2}$ as 2-connected nodes, whereas the 1,3,5-HBTC^{2-} lig-

and is defined as a linker, the structure of **4** can be simplified as a 2,4-connected 1D net with a {4.6^4.8}{4}-2,4C6 topology, as shown in Figure 5b. It is noted that although complexes **1** and **4** adopt the same structural topology of 2,4C6, the 2-connected nodes are 1,3,5-HBTC^{2-} ligands and **L^2** ligands, respectively.

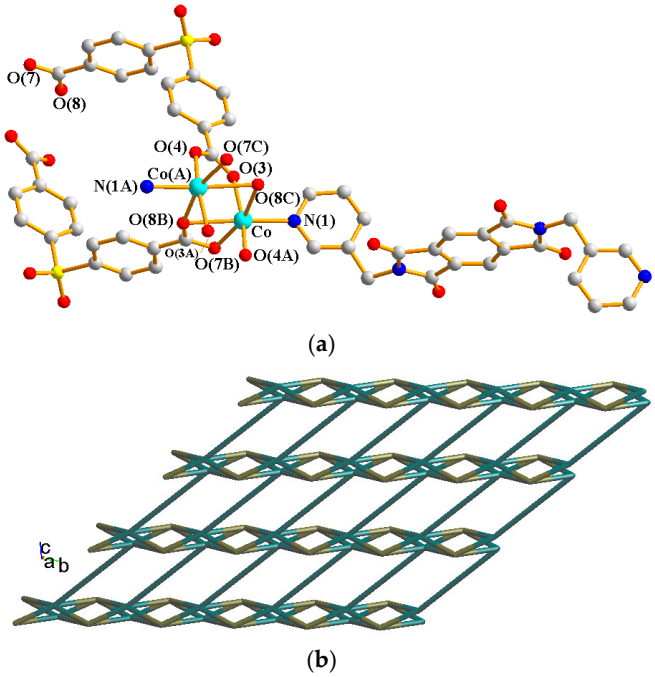


Figure 4. (**a**) Coordination environment around the Co(II) ions of **3**. Symmetry transformations used to generate equivalent atoms: (A) −x + 1, −y − 2, −z + 1; (B) −x + 2, −y − 1, −z + 1; (C) x − 1, y − 1, z. (**b**) A drawing showing the 4,5L51 topology.

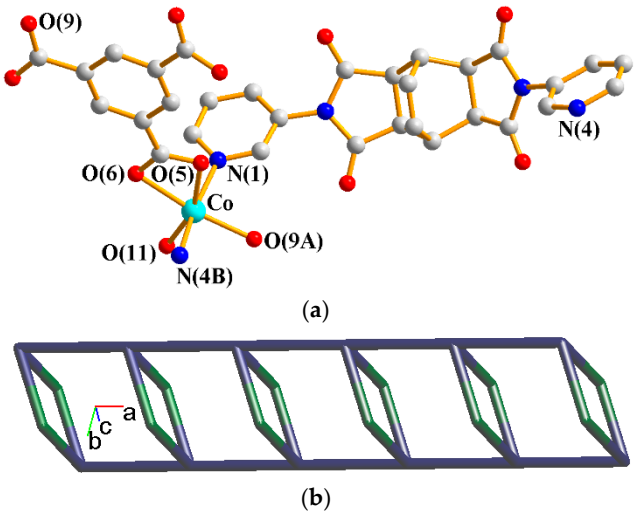


Figure 5. (**a**) Coordination environment about the Co(II) ions of **4**. Symmetry transformations used to generate equivalent atoms: (A) x + 1, y, z; (B) −x + 2, −y + 2, −z + 2; (C) x − 1, y, z. (**b**) A drawing showing the 2,4C6 topology.

2.5. Structure of **5**

The asymmetric unit consists of one Ni(II) cation, one **L^2** ligand, one 1,3,5-HBTC^{2-} ligand, one coordinated water molecule, and one crystallized water molecule. Figure 6a shows the coordination environment around the Ni(II) metal center, which is six-coordinated by two nitrogen atoms from two **L^2** ligands [Ni–N = 2.099(3)–2.114(3) Å], three oxygen atoms from two 1,3,5-HBTC^{2-} ligands [Ni–O = 2.031(2)–2.169(2) Å], and one oxygen

atom from the coordination water molecule [Ni–O = 2.075(2) Å]. The Co(II) cations are linked by 1,3,5-HBTC^{2-} and **L^1** ligands to form 1D chains. If the Co(II) units are defined as 4-connected nodes and **L^2** as 2-connected nodes, whereas the 1,3,5-HBTC^{2-} ligands are defined as the linkers, the structure can be simplified as a 2,4-connected net with a {4.6^4.8}{4}-2,4C6 topology, as shown in Figure 6b.

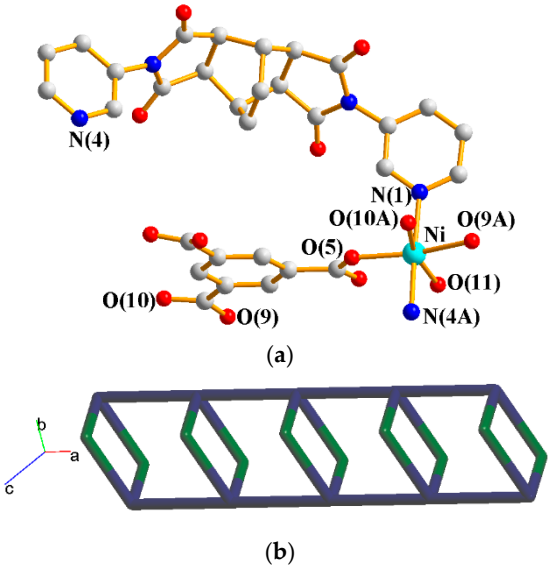


Figure 6. (**a**) Coordination environment about the Ni(II) ions of **5**. Symmetry transformations used to generate equivalent atoms: (A) −x + 1, −y + 1, −z + 1; (B) x − 1, y, z; (C) x + 1, y, z. (**b**) A drawing showing the 2,4C6 topology.

2.6. Structures of **6** *and* **7**

Their asymmetric units consist of a half of a Ni(II) cation, a half of an **L^2** ligand, and a half of an SDA^{2-} or an OBA^{2-} ligand. Figure 7a shows the coordination environment around the Ni(II) metal center of complex **6**, which is six-coordinated by two nitrogen atoms from two **L^2** ligands [Ni–N = 2.099(2) Å] and four oxygen atoms from two SDA^{2-} ligand [Ni–O = 2.0867(17)–2.1923(18) Å]. Figure 7b shows the coordination environment around the Ni(II) metal center of complex **7**, which is six-coordinated by two nitrogen atoms from two **L^2** ligands [Ni–N = 2.0777(18) Å] and four oxygen atoms from two OBA^{2-} ligands [Ni–O = 2.0611(14)–2.1523(15) Å]. Both of the Ni(II) centers of complexes **6** and **7** form distorted octahedral geometries, resulting in 2D layers and the same topological structure. If the Ni(II) ions are defined as 4-connected nodes and the **L^2** and the dicarboxylate (SDA^{2-} and OBA^{2-}) ligands as 2-connected nodes, the structures of **6** and **7** can be simplified as 2,4-connected 2D nets with the {8^4·12^2}{8}$_2$-2,4L2 topology, as shown in Figure 7c. Figure 7d depicts a packing diagram of the 2D layers.

2.7. Ligand Conformations and Coordination Modes

For the **L^1** ligand, the orientations of the two nitrogen atoms of the two pyridyl rings can be distinguished as *cis* or *trans*. It is defined as *trans* when the two nitrogen atoms show opposite directions, and as *cis* when they are of the same. Moreover, *U* and *Z* configurations can be given if the pyridyl rings are pointing to the same and opposite directions, respectively [23,29]. On the other hand, *cis* and *trans* conformations can be applied to the **L^2** ligand if the two pyridyl nitrogen atoms are pointing to the same and opposite directions, respectively. Consequently, the assigned ligand conformations of **L^1** and **L^2** of complexes **1**–**7** are listed in Table 1. The coordination modes of the polycarboxylate ligands in Table 1 indicate that these ligands bridge two and four metal ions. For comparisons, it is noted that in the two CPs, {[Hg(3-pmpmd)I$_2$]·H$_2$O)}$_n$, {[Ni$_2$(3-pmpmd)$_3$(NO$_3$)$_4$]·2CH$_3$OH}$_n$, two

types of ligand conformations, Z_T and U_C, are observed for the 3-pmpmd (**L**^{1}) ligands [34]. On the other hand, all the 3-pmpmd (**L**^{1}) ligands in the supramolecular compounds, $\{[3\text{-pmpmd}]\}_n$, $\{H_2[3\text{-pmpmd}]\cdot 2NO_3^-\}_n$ and $\{H_2[3\text{-pmpmd}]\cdot 2tbb\}_n$ (tbb = tertiary butyl benzoic acid) afforded the Z_T conformation [35].

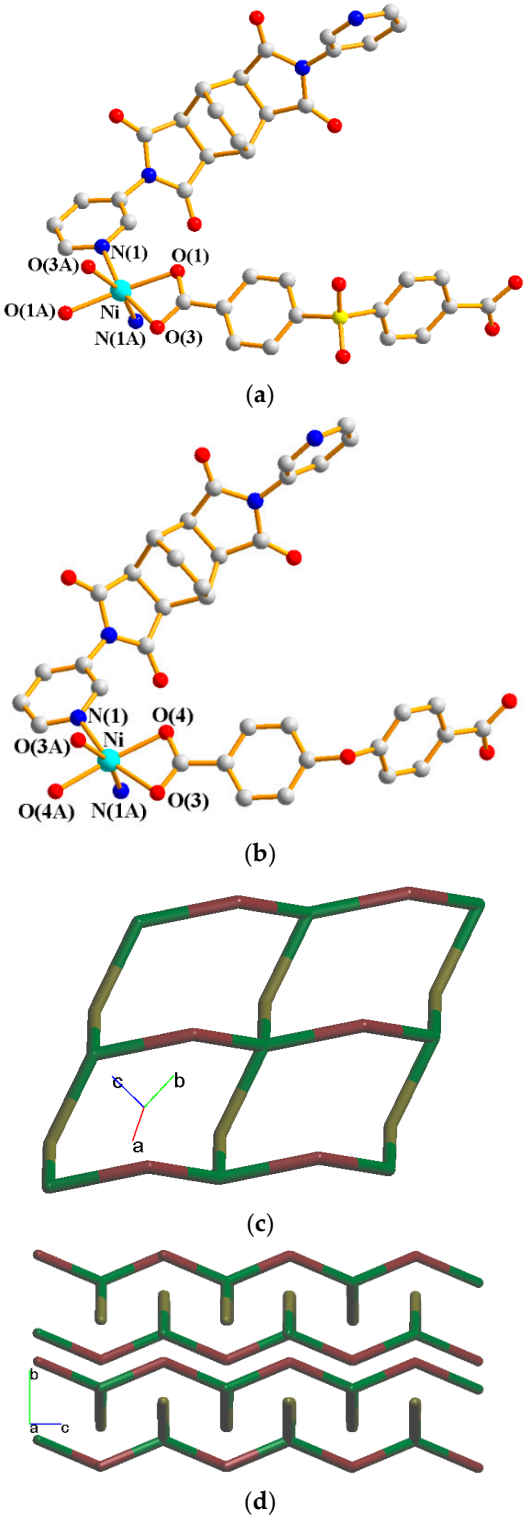
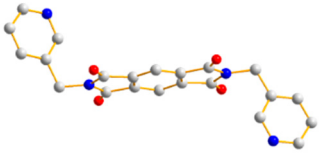
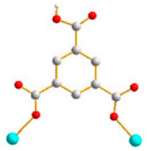
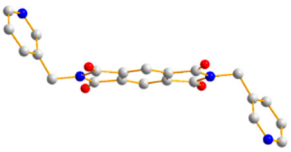
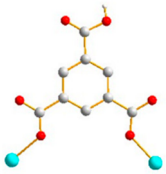
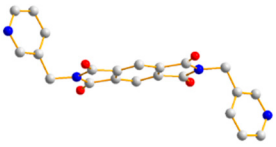
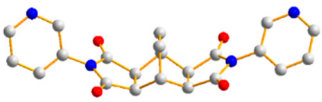
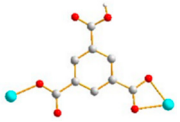
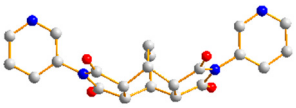
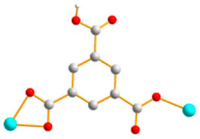
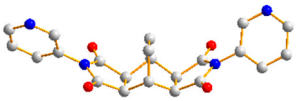
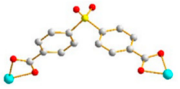
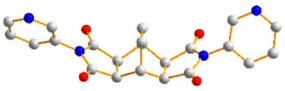
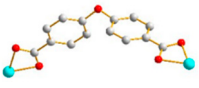


Figure 7. (**a**) Coordination environment around the Ni(II) ions of **6**. Symmetry transformations used to generate equivalent atoms: (A) x + 1, y, −z + 1/2; (B) −x + 2, y, −z + 3/2; (C) −x + 2, y, −z + 1/2. (**b**) Coordination environment around the Ni(II) ions of **7**. Symmetry transformations used to generate equivalent atoms: (A) −x, y, −z + 1/2; (B) −x + 1, y, −z + 3/2; (C) −x + 1, y, −z + 1/2. (**c**) A drawing showing the 2,4L2 topology. (**d**) A packing diagram of the 2D layers.

2.8. Powder X-Ray Analysis

To check the phase purity of the products, powder X-ray diffraction (PXRD) experiments were performed for all complexes. As shown in Figures S1–S7, the peak positions of the experimental and simulated PXRD patterns are in good agreement with each other, suggesting the good bulk purities of these CPs.

Table 1. Ligand conformations and bonding modes of complexes **1**–**7**.

	Ligand Conformation	Coordination Mode
1	 Z_T	 μ_2-κ*O*:κ*O*′
2	 Z_T	 μ_2-κ*O*:κ*O*′
3	 Z_T	 μ_4-κ^2*O*,*O*′:κ*O*″:κ*O*‴:κ*O*⁗
4	 *cis*	 μ_2-κ^2*O*,*O*′:κ*O*″
5	 *cis*	 μ_2-κ^2*O*,*O*′:κ*O*″
6	 *cis*	 μ_2-κ^2*O*,*O*′:κ^2*O*″,*O*‴
7	 *cis*	 μ_2-κ^2*O*,*O*′:κ^2*O*″,*O*‴

2.9. Thermal Properties

The thermal decompositions of the CPs were examined by using thermal gravimetric analyses (TGAs), which were executed under nitrogen gas at a pressure of 1 atm with a heating rate of 10 °C min^{-1}. Table 2 and Figures S8–S14 show that the complexes **1**–**5** suffered two-step decomposition involving the loss of solvent molecules and loss of organic ligands, whereas **6** and **7** only experienced the loss of organic ligands.

2.10. Gas Adsorption

Using the PLATON program [36], the solvent-accessible volumes of the complexes **1**–**7** were estimated, giving 3.7, 0, 9.1, 0, 10.5, 1.8, and 1.0% of the corresponding unit cell volumes, respectively. Since the yield of complex **1** is low and **2** and **4** show zero solvent-accessible volume, the N_2 gas adsorption complexes **3**, **5**, **6,** and **7** were thus investigated for the further iodine adsorption experiments. The N_2 adsorption measurements were performed at 1.0 bar and 77 K, and the complexes were heated at 120 °C for 24 h to obtain fully activated ones before the measurements, affording BET surface areas of 9.25, 62.11, 13.3, and 10.28 m^2/g, and N_2 uptake capacities of 8.62, 42.76, 11.94, and 8.70 cm^3/g for complexes **3**, **5**, **6,** and **7**, respectively, as shown in Figures S15–S18. The pore-size distribution curves show that the pore sizes of complexes **3**, **5**, **6,** and **7** are 5.96, 7.57, 5.86, and 6.84 nm, respectively, as shown in Figures S19–S22. The results indicate that complex **5** has the best surface area and N_2 uptake capacity. Figures S23–S26 demonstrate that the complexes remain stable after gas adsorption.

Table 2. Thermal properties of complexes **1**–**7**.

Complex	Weight Loss of Solvent °C (Calc/Found),%	Weight Loss of Ligand °C (Calc/Found),%
1	2 H_2O 30–175 (7.50/11.01)	$\mathbf{L^1}$ + 1,3,5-$HBTC^{2-}$ 175–650 (84.31/80.24)
2	4 H_2O 30–170 (13.37/11.00)	0.5 ($\mathbf{L^1}$) + 1,3,5-$HBTC^{2-}$ 170–540 (75.69/71.97)
3	1 H_2O 30–345 (3.10/6.66)	0.5 ($\mathbf{L^1}$) + SDA^{2-} 345–550 (86.79/83.48)
4	2 H_2O 30–230 (5.10/5.17)	$\mathbf{L^2}$ + 1,3,5-$HBTC^{2-}$ 230–540 (86.55/85.06)
5	2 H_2O 30–260 (5.11/5.23)	$\mathbf{L^2}$ + 1,3,5-HBC^{2-}) 260–800 (87.83/86.55)
6		$\mathbf{L^2}$ + SDA^{2-} 30–800 (92.32/91.10)
7		$\mathbf{L^2}$ + OBA^{2-} 30–600 (91.80/92.45)

2.11. Iodine Adsorption

The iodine adsorption capabilities of complexes **3**, **5**, **6,** and **7** were investigated at 35 and 75 °C with time intervals of 0.5, 1, 2, 3, 4, 5, 6, 12, 24, 36, and 48 h. Each experiment was repeated three times and performed by heating the apparatus involving 10 mg of each complex in a smaller sample bottle (4 mL) inside a larger one (20 mL) having 1 g of iodine. The changes in the colors of the complexes at 35 and 75 °C are shown in Figures S27–S34.

Tables S1–S8 summarize the results for I_2 adsorption, while Figures 8 and 9 display the average iodine vapor adsorption rates of complexes **3**, **5**, **6,** and **7** at 35 and 75 °C, showing that the adsorption rate has a strong dependence on temperature and the best adsorption capacity is 133.77 mg g^{-1} at 75 °C for 24 h, as observed in **3**. The results indicate that the surface area and N_2 uptake capacity of the complexes investigated may not govern the iodine adsorptions. PXRD patterns were measured to evaluate the structures of the iodine-adsorbed samples, as shown in Figures S35–S42, demonstrating that the iodine-adsorbed samples probably retain the structures of complexes **3**, **5**, **6,** and **7**.

2.12. Recyclability

The recyclability and reusability of adsorbents are also very important in industrial applications. The iodine-adsorbed samples were placed in ethanol for 24 h to eradicate the iodine, and the ethanol was replaced with fresh ethanol every 8 h. Figures S43–S46

show the PXRD patterns of the CPs upon I_2 removal, indicating no significant structural changes. The desorbed CPs were then heated to 120 °C for 24 h and then subjected to iodine adsorption again. After four cycles, the adsorption capabilities of complexes **3**, **5**, **6**, and **7** were evaluated, giving 66.42, 85.25, 94.62, and 56.07% of their original ones, respectively, as shown in Figure 10. Figures S47–S50 show that these CPs remain stable after four cycles.

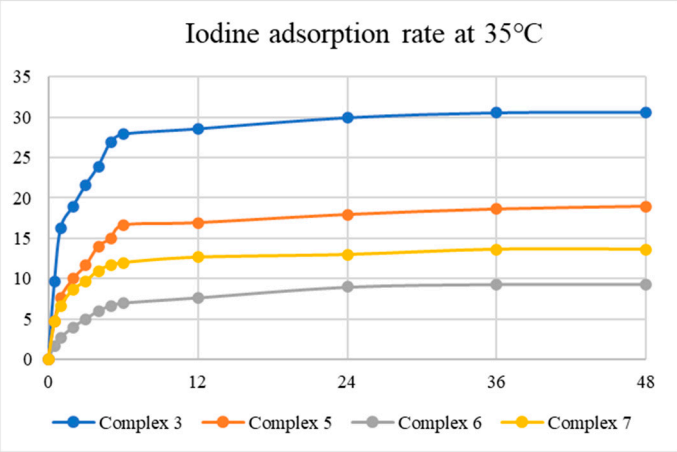


Figure 8. Iodine vapor adsorption rate of the complexes at 35 °C.

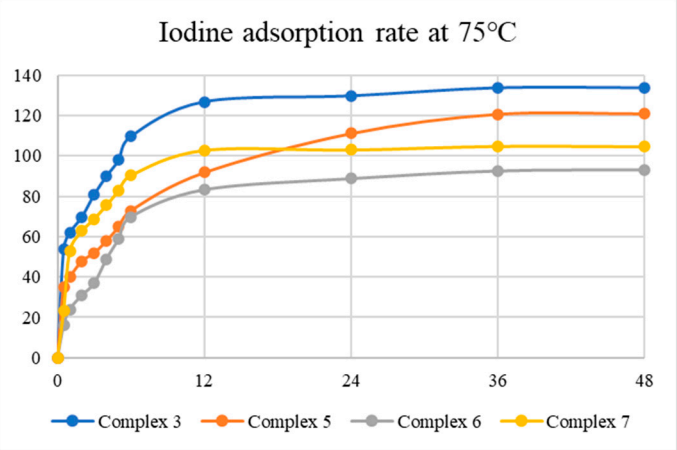


Figure 9. Iodine vapor adsorption rate of the complexes at 75 °C.

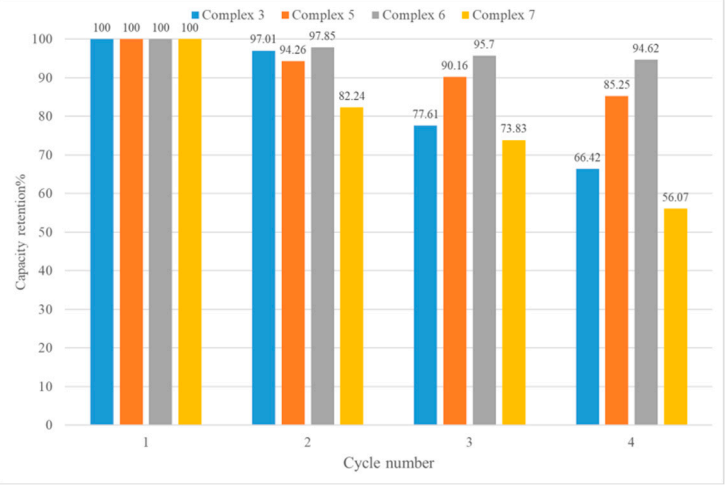


Figure 10. Capacity retention of complexes after several I_2 vapor adsorption/desorption cycles.

2.13. X-Ray Photoelectron Spectroscopy (XPS)

X-ray photoelectron spectroscopy (XPS) was applied to investigate the interaction between the complex and iodine [37,38]. The XPS broad spectra, shown in Figures S51–S54, reveal peaks of I $3d_{3/2}$, I $3d_{5/2}$, and I 4d for the iodine-adsorbed **3**, **5**, **6,** and **7**, respectively, confirming the adsorption of iodine by the four CPs. The spectra given in Figures S55–S58 indicate that each of I $3d_{3/2}$ and I $3d_{5/2}$, centered at ~631 and ~619 eV, can be fitted into two peaks, assignable to I_2 and I_3^-, respectively. Specifically, the peaks are attributed to I_2 (631.1 eV; 619.9 eV) and I_3^- (630.1 eV; 618.7 eV) for **3**, (631.0 eV; 619.4 eV) and (630.0 eV; 618.6 eV) for **5**, (631.1 eV; 619.8 eV) and (630.1 eV; 618.7 eV) for **6**, and (630.9 eV; 619.5 eV) and (630.0 eV; 618.5 eV) for **7**, respectively.

The XPS N1s spectra of the original complexes and the iodine-adsorbed samples show obvious changes in binding energy, indicating the electron transfer from N to I atoms, as shown in Figures S59–S62. Figures S63–S66 give the XPS spectra of C1s for the four CPs before and after iodine capture, which are fitted with five peaks and the peak around 288 eV corresponds to the C=O. It is evident that these peaks exhibit significant blue shifts upon iodine adsorption, probably due to the interactions between iodine and the oxygen atoms of the C=O, causing the electrons on carbon atoms to be pulled toward oxygen atoms and leading to blue shifts in the binding energies of C1s.

Interestingly, the peak areas assignable to sp^2 C-C become smaller after iodine adsorption, although the binding energies do not change significantly. Specifically, the area of complex **3** dropped from 35.20 to 20.21%, while those of complexes **5**–**7** dropped from 20.56 to 12.16%, 10.04 to 6.01%, and 9.73 to 2.94%, respectively, with increasing intensities of the other three peaks. This suggests that the iodine-interacted C-C sp^2 peak may overlap with the other three peaks and thereby increase their peak areas. The most significant change (about 15%) in the C-C sp^2 peak area is observed in complex **3**, which may be attributed to the interaction of the pi electrons of the $\mathbf{L^1}$ ligand with iodine. Moreover, the better adsorption rate of complex **3** may indicate that the π conjugation system of the $\mathbf{L^1}$ ligand forms stronger donor–acceptor interactions with the iodine molecules than the $\mathbf{L^2}$ ligands of complexes **5**–**7** with a single double bond in the center of the spacer. The XPS results thus suggest that the adsorption mechanism likely involves the transfer of π electrons from $\mathbf{L^1}$ and $\mathbf{L^2}$ to I_2, forming polyiodides.

3. Experimental Section

3.1. General Procedures

Elemental analyses of (C, H, N) were performed on a PE 2400 series II CHNS/O (PerkinElmer Instruments, Shelton, CT, USA) or an Elementar Vario EL-III analyzer (Elementar Analysensysteme GmbH, Hanau, Germany). Infrared spectra were obtained from a JASCO FT/IR-460 plus spectrometer with pressed KBr pellets (JASCO, Easton, MD, USA). Gas sorption measurements were conducted using a Micromeritics ASAP 2020 system (Micromeritics Instruments Co., Norcross, GA, USA). Powder X-ray diffraction patterns were carried out with a Bruker D8-Focus Bragg–Brentano X-ray powder diffractometer equipped with a CuKα ($\lambda\alpha$ = 1.54178 Å) sealed tube (Bruker Corporation, Karlsruhe, Germany). X-ray photoelectron spectroscopy (XPS) was on performed on a PHI Quantes spectrometer (Ulvac-Phi Inc., Kanagawa, Japan).

3.2. Materials

The reagents $Ni(OAc)_2{\cdot}4H_2O$ and 1,3,5-H_3BTC were purchased from Alfa Aesar Co. (Ward Hill, MA, USA), $Co(OAc)_2{\cdot}4H_2O$ from J. T. Baker Co. (Phillipsburg, NJ, USA), H_2SDA and H_2OBA from Aldrich Chemical Co. (St. Louis, MO, USA). The ligand *N,N′*-bis(3-pyridylmethyl)-pyromellitic diimide ($\mathbf{L^1}$) [24] and *N,N′*-bis(3-pyridyl)bicyclo(2,2,2,)oct-

7-ene-2,3,5,6-tetracarboxylic diamide(**L²**) [25,26] were prepared according to published procedures. Complexes **2**–**7** were prepared by following similar procedures for **1**.

3.3. Preparations

3.3.1. {[Co(**L¹**)(1,3,5-HBTC)(H_2O)$_2$]·H_2O}$_n$, **1**

A mixture of Co(OAc)$_2$·4H_2O (0.025 g, 0.10 mmol), **L¹** (0.030 g, 0.10 mmol), and 1,3,5-H_3BTC (0.021 g, 0.10 mmol) in 10 mL H_2O was sealed and heated in an autoclave to 100 °C for two days, which was then cooled to room temperature at a rate of 2 °C per hour. Suitable pink crystals were prepared. Yield: 0.0080 g (11%). Anal. Calcd for $C_{31}H_{24}CoN_4O_{13}$ (MW = 719.47): C, 51.75; H, 3.36; N,7.78%. Found: C, 48.40; H, 3.25; N, 6.77%. IR (cm^{-1}): 3439(m), 3006(m), 1776(m), 1703(s), 1608(s), 1576(m), 1433(m), 1394(s), 1303(m), 1272(m), 1095(m), 924(m), 759(m), 706(m).

3.3.2. {[Co(**L¹**)$_{0.5}$(1,3,5-HBTC)(H_2O)$_3$]·H_2O}$_n$, **2**

A mixture of Co(OAc)$_2$·4H_2O (0.075 g, 0.30 mmol), **L¹** (0.030 g, 0.10 mmol) and 1,3,5-H_3BTC (0.042 g, 0.20 mmol) 10 mL H_2O was used. Pink crystals were obtained. Yield: 0.0134 g (8%). Anal. Calcd for $C_{20}H_{19}CoN_2O_{12}$ (MW = 538.30): C, 44.62; H, 3.55; N, 5.20%. Found: C, 44.05; H, 3.39; N, 5.51%. IR (cm^{-1}):3342(m), 3097(m), 1769(m), 1703(s), 1604(s), 1483(w), 1434(m), 1395(s), 1094(m), 1278(w), 1171(w), 1072(w), 926(m), 784(w), 734(m).

3.3.3. {[Co(**L¹**)$_{0.5}$(SDA)]·H_2O}$_n$, **3**

A mixture of Co(OAc)$_2$·4H_2O (0.025 g, 0.10 mmol), **L¹** (0.030 g, 0.10 mmol) and H_2SDA (0.031 g, 0.10 mmol) 10 mL H_2O was used. Suitable dark pink crystals were obtained. Yield: 0.027 g (54%). Anal Calcd for $C_{25}H_{17}CoN_2O_9S$ (MW = 580.39): C, 53.39; H, 2.68; N, 4.98%. Found: C, 53.36; H, 2.72; N, 5.37%. IR (cm^{-1}): 3262(s), 2978(w), 2934(w), 2361(m), 1772(m), 1725(s), 1611(s), 1563(m), 1487(m), 1417(s), 1392(s), 1358(m), 1290(m), 1191(w), 1159(m), 1100(m), 1065(w), 1010(w), 963(w), 943(w), 922(w), 874(w), 851(w), 780(m), 742(s).

3.3.4. {[Co(**L²**)(1,3,5-HBTC)(H_2O)]·H_2O}$_n$, **4**

A mixture of Co(OAc)$_2$·4H_2O (0.075 g, 0.30 mmol), **L²** (0.040 g, 0.10 mmol) and 1,3,5-H_3BTC (0.042 g, 0.20 mmol) 10 mL H_2O was used. Purple crystals were obtained. Yield: 0.0126 g (6%). Anal. Calcd for $C_{62}H_{52}Co_2N_8O_{24}$ (MW = 1410.97): C, 52.77; H, 3.71; N, 7.94%. Found: C, 52.61; H, 3.19; N, 8.17%. IR (cm^{-1}): 2937(s), 1709(s), 1619(s), 1539(m), 1484(m), 1437(s), 1378(s), 1270(w), 1237(w), 1183(s), 1103(w), 929(w), 780(m), 727(m), 696(m), 590(w).

3.3.5. {[Ni(**L²**)(1,3,5-HBTC)·H_2O]·H_2O}$_n$, **5**

A mixture of Ni(OAc)$_2$·4H_2O (0.025 g, 0.10 mmol), **L²** (0.040 g, 0.10 mmol) and 1,3,5-H_3BTC (0.021 g, 0.10 mmol) 10 mL H_2O was used. Blue crystals were obtained. Yield: 0.043 g (56%). Anal Calcd for $C_{31}H_{24}NiN_4O_{12}$ (MW = 703.25): C, 52.94; H, 3.43; N,7.96%. Found: C, 52.14; H, 3.67; N, 7.87%. IR (cm^{-1}): 3350(s), 3070(m), 2361(w), 1175(m), 1708(s), 1614(m), 1566(m), 1533(m), 1485(m), 1455(w), 1435(m), 1373(s), 1311(m), 1035(w), 930(w), 874(w), 778(s), 756(m), 726(m).

3.3.6. [Ni(**L²**)(SDA)]$_n$, **6**

A mixture of Ni(OAc)$_2$·4H_2O (0.025 g, 0.10 mmol), **L²** (0.040 g, 0.10 mmol) and H_2SDA (0.031 g, 0.10 mmol) 10 mL H_2O was used. Green crystals were obtained. Yield: 0.052 g (74%). Anal Calcd for $C_{36}H_{24}NiN_4O_{10}S$ (MW = 763.36): C, 56.64; H, 3.16; N, 7.33%. Found: C, 56.39; H, 2.89; N, 7.69%. IR (cm^{-1}): 3398(s), 3061(w), 2360(w), 1776(m),

1720(s), 1532(s), 1485(m), 1417(m), 1379(s), 1321(m), 1296(m), 1237(w), 1183(s), 1159(m), 1100(m), 1012(w), 881(w), 859(m), 776(m), 751(s), 695(m), 648(w), 618(m), 586(w), 538(w).

3.3.7. $[Ni(\mathbf{L^2})(OBA)]_n$, **7**

A mixture of $Ni(OAc)_2{\cdot}4H_2O$ (0.050 g, 0.20 mmol), $\mathbf{L^2}$ (0.040 g, 0.10 mmol) and H_2OBA (0.026 g, 0.10 mmol) 10 mL H_2O was used. Green crystals were obtained. Yield: 0.021 g (14%). Anal Calcd for $C_{36}H_{24}NiN_4O_9$ (MW = 715.30): C, 60.44; H, 3.38; N, 7.83%. Found: C, 60.39; H, 3.20; N, 7.58%. IR (cm^{-1}): 3390(s), 3060(w), 2360(w), 1775(m), 1720(s), 1590(s), 1528(m), 1484(m), 1438(s), 1382(s), 1351(m), 1304(w), 114(s), 1183(s), 1159(m), 1094(w), 1012(w), 876(m), 778(m), 700(m), 652(m).

3.4. X-Ray Crystallography

The crystal data of complexes **1–7** were collected by using a Bruker AXS SMART APEX II CCD diffractometer at 100 or 298 K and data reduction was achieved by using standard methods [39]. While some heavier atoms were located by direct or Patterson methods and the remaining atoms by a series of alternating difference Fourier maps and least-square refinements, the hydrogen atoms except those of the water molecules were added by using the HADD command in SHELXTL 6.1012 [40]. CCDC nos. 2410834–2410840 contain the supplementary crystallographic data for complexes **1–7** and Table 3 lists their crystal data.

Table 3. Crystal data for complexes **1–7**.

Complex	**1**	**2**	**3**	**4**
CCDC No.	2410834	2410835	2410836	2410837
Formula	$C_{31}H_{24}CoN_4O_{13}$	$C_{20}H_{19}CoN_2O_{12}$	$C_{25}H_{17}CoN_2O_9S$	$C_{62}H_{52}CoN_8O_{24}$
Formula weight	719.47	538.30	580.39	1410.97
Crystal system	Triclinic	Monoclinic	Triclinic	Triclinic
Space group	$P\bar{1}$	$P2_1/c$	$P\bar{1}$	$P\bar{1}$
a, Å	9.156(7)	10.8982(5)	8.4917(9)	10.3096(7)
b, Å	13.754(9)	20.3062(8)	12.0705(12)	11.9016(8)
c, Å	14.239(10)	11.0603(5)	12.3303(13)	12.3186(9)
α, °	105.32(2)	90	95.326(3)	92.5130(18)
β, °	105.84(2)	119.3790(10)	100.465(3)	99.3631(18)
γ,°	105.05(3)	90	100.273(3)	96.1909(16)
V, $Å^3$	1553.9(19)	2132.87(16)	1212.6(2)	1479.76(18)
Z	2	4	2	1
D_{calc}, Mg/m^3	1.538	1.676	1.590	1.583
F(000)	738	1104	592	726
μ(Mo K_α), mm^{-1}	0.100	0.100	0.100	0.100
Range(2θ) for data collection, deg	$3.18 \leq 2\theta \leq 52.00$	$4.01 \leq 2\theta \leq 56.67$	$3.38 \leq 2\theta \leq 51.99$	$3.35 \leq 2\theta \leq 52.00$
Independent reflection	6112 [R(int) = 0.0711]	5306 [R(int) = 0.0392]	4776 [R(int) = 0.0460]	5833 [R(int) = 0.1011]
Data/restraint/parameter	6112/0/442	5306/0/316	4766/0/342	5833/0/443
quality-of-fit indicator [c]	1.019	1.014	1.019	1.021
Final R indices [I > 2σ(I)] [a,b]	R_1 = 0.0566, wR_2 = 0.1366	R_1 = 0.0376, wR_2 = 0.0800	R_1 = 0.0386, wR_2 = 0.0861	R_1 = 0.0615, wR_2 = 0.1417
R indices (all data)	R_1 = 0.0922, wR_2 = 0.1555	R_1 = 0.0659, wR_2 = 0.0906	R_1 = 0.0555, wR_2 = 0.0944	R_1 = 0.1293, wR_2 = 0.1729

Table 3. *Cont.*

Complex	5	6	7
CCDC No.	2410838	2410839	2410840
Formula	$C_{31}H_{24}N_4NiO_{12}$	$C_{36}H_{24}N_4NiO_{10}S$	$C_{36}H_{24}N_4NiO_9$
Formula weight	703.25	763.36	715.30
Crystal system	Monoclinic	Monoclinic	Monoclinic
Space group	$P2_1/c$	$C2/c$	$C2/c$
a, Å	10.298(3)	12.902(5)	12.9670(7)
b, Å	12.219(3)	20.793(7)	19.6947(11)
c, Å	14.6033(2)	13.180(4)	12.9964(10)
α, °	25.655(7)	90	90
β, °	90	111.607(9)	113.6724(12)
γ,°	96.424(5)	90	90
V, Å^3	90	3287(2)	3039.8(3)
Z	4	4	4
D_{calc}, Mg/m^3	1.456	1.542	1.563
F(000)	1448	1568	1472
μ(Mo K_α), mm^{-1}	0.100	0.100	0.100
Range (2θ) for data collection, deg	$3.19 \leq 2\theta \leq 52.00$	$3.91 \leq 2\theta \leq 52.00$	$1.00 \leq 2\theta \leq 52.00$
Independent reflection	6308 [R(int) =0.0532]	3229 [R(int) = 0.0400]	2989 [R(int) = 0.0471]
Data/restraint/parameter	6308/0/446	3229/0/236	2989/0/243
quality-of-fit indicator [c]	1.050	1.026	1.016
Final R indices [$I > 2\sigma(I)$] [a,b]	R_1 = 0.0531, wR_2 = 0.1486	R_1 = 0.0368, wR_2 = 0.0787	R_1 = 0.0345, wR_2 = 0.0659
R indices (all data)	R_1 = 0.0707, wR_2 = 0.1620	R_1 = 0.0567, wR_2 = 0.0858	R_1 = 0.0557, wR_2 = 0.0725

[a] $R_1 = \Sigma||F_o| - |F_c||/\Sigma|F_o|$. [b] $wR_2 = [\Sigma w(F_o^2 - F_c^2)^2/\Sigma w(F_o^2)^2]^{1/2}$. $w = 1/[\sigma^2(F_o^2) + (ap)^2 + (bp)]$, $p = [\max(F_o^2 \text{ or } 0) + 2(F_c^2)]/3$. a = 0.0856, b = 0.1326 for 1; 0.0400, b = 0.5411 for 2; a = 0.0344, b = 1.1152 for 3; a = 0.0787, b = 1.1807 for 4; a = 0.0902, b = 4.8786 for 5; a = 0.0357, b = 2.8433 for 6; a = 0.0247, b = 2.7813 for 7. [c] quality-of-fit = $[\Sigma w(|F_o^2| - |F_c^2|)^2/(N_{observed} - N_{parameters})]^{1/2}$.

4. Conclusions

Seven 1D and 2D non-entangled CPs based on the semi-rigid spacer ligands **L^1** and **L^2** have been successfully obtained, which indirectly demonstrates that the flexible nature of the bpba ligand may govern the formation of the entangled CPs. The rigidity thus hinders the spacer ligands from adjusting the steric requirements for the formation of the entangled CPs. The iodine adsorption studies of complexes **3**, **5**, **6,** and **7** show that **3** gives a better iodine-adsorption factor of 133.77 mg g^{-1} at 75 °C for 24 h than the others, confirming that the π conjugated system of **L^1** may enhance the capacity of iodine adsorption, although the metal identity may play some role.

Supplementary Materials: The following supporting information can be downloaded at: https://www.mdpi.com/article/10.3390/inorganics13030069/s1, Powder X-ray patterns (Figures S1–S7, S23–S26, S35–S50). TGA curves (Figures S8–S14). N_2 adsorption−desorption isotherms (Figures S15–S18). Pore-size distribution curve (Figures S19–S22). Color changes (Figures S27–S34). Table of Iodine adsorption experiments (Tables S1–S8). XPS spectra (Figures S52–S66). Crystallographic data for complexes **1**–**7** have been deposited with the Cambridge Crystallographic Data Centre, CCDC No. 2410834–2410840.

Author Contributions: Investigation, Y.-W.C.; data curation, Z.-L.C. and S.-W.W.; review and supervision, J.-D.C. All authors have read and agreed to the published version of the manuscript.

Funding: This research was funded by the National Science and Technology Council of the Republic of China: NSTC 112-2113-M-033-004.

Data Availability Statement: Data are contained within the article or Supplementary Materials.

Acknowledgments: We are grateful to the National Science and Technology Council of the Republic of China for support.

Conflicts of Interest: The authors declare no conflicts of interest.

References

1. Batten, S.R.; Champness, N.R.; Chen, X.-M.; Martinez, J.G.; Kitagawa, S.; Öhrström, L.; Keeffe, M.O.; Suh, M.P.; Reedijk, J. Terminology of metal–organic frameworks and coordination polymers (IUPAC Recommendations 2013). *Pure Appl. Chem.* **2013**, *85*, 1715–1724. [CrossRef]
2. Li, M.; Li, D.; O'Keeffe, M.; Yaghi, O.M. Topological Analysis of Metal–Organic Frameworks with Polytopic Linkers and/or Multiple Building Units and the Minimal Transitivity Principle. *Chem. Rev.* **2014**, *114*, 1343–1370. [CrossRef]
3. Wales, D.J.; Grand, J.; Ting, V.P.; Burke, R.D.; Edler, K.J.; Bowen, C.R.; Mintova, S.; Burrows, A.D. Gas sensing using porous materials for automotive applications. *Chem. Soc. Rev.* **2015**, *44*, 4290–4321. [CrossRef] [PubMed]
4. Li, J.-R.; Sculley, J.; Zhou, H.-C. Metal–Organic Frameworks for Separations. *Chem. Rev.* **2012**, *112*, 869–932. [CrossRef] [PubMed]
5. Lustig, W.P.; Mukherjee, S.; Rudd, N.D.; Desai, A.V.; Li, J.; Ghosh, S.K. Metal–organic frameworks: Functional luminescent and photonic materials for sensing applications. *Chem. Soc. Rev.* **2017**, *46*, 3242–3285. [CrossRef] [PubMed]
6. Safarifard, V.; Morsali, A. Influence of an amine group on the highly efficient reversible adsorption of iodine in two novel isoreticular interpenetrated pillared-layer microporous metal–organic frameworks. *CrystEngComm* **2014**, *16*, 8660–8663. [CrossRef]
7. Guo, B.; Li, F.; Wang, C.; Zhang, L.; Sun, D. A rare (3,12)-connected zirconium metal–organic framework with efficient iodine adsorption capacity and pH sensing. *J. Matter. Chem. A.* **2019**, *7*, 13173–13179. [CrossRef]
8. Ju, Y.; Li, Z.J.; Lu, H.; Zhou, Z.; Li, Y.; Wu, X.L.; Guo, X.; Qian, Y.; Zhang, Z.H.; Lin, J.; et al. Interpenetration Control in Thorium Metal-Organic Frameworks: Structural Complexity toward Iodine Adsorption. *Inorg. Chem.* **2021**, *60*, 5617–5626. [CrossRef] [PubMed]
9. Arici, M.; Yeşilel, O.Z.; Taş, M.; Demiral, H. CO_2 and Iodine Uptake Properties of Co(II)-Coordination Polymer Constructed from Tetracarboxylic Acid and Flexible Bis(imidazole) Linker. *Cryst. Growth Des.* **2017**, *17*, 2654–2659. [CrossRef]
10. Mondal, S.; Dastidar, P. Mixed Ligand Coordination Polymers for Metallogelation and Iodine Adsorption. *Cryst. Growth Des.* **2019**, *19*, 470–478. [CrossRef]
11. Liu, J.H.; Qi, Y.J.; Zhao, D.; Li, H.H.; Zheng, S.T. Heterometallic Organic Frameworks Built from Trinuclear Indium and Cuprous Halide Clusters: Ligand-Oriented Assemblies and Iodine Adsorption Behavior. *Inorg. Chem.* **2019**, *58*, 516–523. [CrossRef] [PubMed]
12. Lee, W.-T.; Liao, T.-T.; Chen, J.-D. Nickel(II) Coordination Polymers Supported by Bis-pyridyl-bis-amide and Angular Dicarboxylate Ligands: Role of Ligand Flexibility in Iodine Adsorption. *Int. J. Mol. Sci.* **2022**, *23*, 3603. [CrossRef]
13. Hu, J.-H.; Liu, Y.-C.; Liu, Y.-H.; Chen, J.-D. Structural transformations in cobalt(ii) coordination polymers constructed from flexible N, N′-bis (3-pyridylmethyl) sebacoamide and benzene-1, 3, 5-tricarboxylic acid. *CrystEngComm* **2022**, *24*, 4120–4127. [CrossRef]
14. Chen, W.-J.; Lee, C.-Y.; Huang, Y.-H.; Chen, J.-D. Cd(II) and Co(II) coordination polymers constructed from N,N′-Bis(3-pyridylmethyl)oxalamide and 1,4-Naphthalenedicarboxylic acid. *Polyhedron* **2022**, *223*, 115991. [CrossRef]
15. Zhou, G.-L.; Liu, B.-W.; Cui, G.-Y.; Zhang, W.; Yang, J.-M. Highly efficient iodine capture from vapor and water using UiO-66-X: Effects of functional group modifications. *Inorg. Chim. Acta* **2025**, *575*, 122419. [CrossRef]
16. Liu, Y.; Tan, C.; Li, X.; Jia, Y.; Zhu, L.; Li, Z.; Liu, W. Deposition of Imidazole into Mesoporous Zirconium Metal−Organic Framework for Iodine Capture. *Inorg. Chem.* **2024**, *63*, 21541–21547. [CrossRef] [PubMed]
17. Zaguzin, A.S.; Sukhikh, T.S.; Kolesov, B.A.; Sokolov, M.N.; Fedin, V.P.; Adonin, S.A. Iodinated vs non-iodinated: Comparison of sorption selectivity by $[Zn_2(bdc)_2dabco]_n$ and superstructural 2-iodoterephtalate-based metal–organic framework. *Polyhedron* **2022**, *212*, 115587. [CrossRef]
18. Zhang, X.; Silva, I.D.; Fazzi, R.; Sheveleva, A.M.; Han, X.; Spencer, B.F.; Sapchenko, S.A.; Tuna, F.; McInnes, E.J.L.; Li, M.; et al. Iodine Adsorption in a Redox-Active Metal−Organic Framework:Electrical Conductivity Induced by Host−Guest Charge-Transfer. *Inorg. Chem.* **2019**, *58*, 14145–14150. [CrossRef] [PubMed]
19. Barsukova, M.O.; Sapchenko, S.A.; Kovalenko, K.A.; Samsonenko, D.G.; Potapov, A.S.; Danil, N.; Dybtsev, D.N.; Fedinab, V.P. Exploring the multifunctionality in metal–organic framework materials: How do the stilbenedicarboxylate and imidazolyl ligands tune the characteristics of coordination polymers? *New J. Chem.* **2018**, *42*, 6408. [CrossRef]

20. Zaguzin, A.S.; Mahmoudi, G.; Sukhikh, T.S.; Sakhapov, I.F.; Zherebtsov, D.A.; Zubkov, F.; Valchuk, K.S.; Sokolov, M.N.; Fedin, V.P.; Adonin, S.A. 2D and 3D Zn(II) coordination polymers based on 4 -(Thiophen-2-yl)-4,2′:6′,4 ′-terpyridine: Structures and features of sorption behavior. *J. Mol. Struct.* **2022**, *1255*, 132459. [CrossRef]
21. Khan, M.-M.; Chen, K.-W.; Chen, Y.-T.; Liu, H.-Y.; Xia, M.; Ni, F.; Gong, C.-H.; Wang, P.; Yang, Y. A highly efficient composite of Cu-BTC and g-C3N4 with bismuth doped for the adsorption of radioactive iodine. *Sep. Purif. Technol.* **2025**, *354*, 128746. [CrossRef]
22. Chanda, A.; Mandal, S.K. Two Metal−Organic Frameworks with a Fused Cis-Decalin Conformation for Multimedia Iodine Capture. *Inorg. Chem.* **2024**, *63*, 13367–13379. [CrossRef] [PubMed]
23. Huang, W.-C.; Chen, W.-H.; Chen, C.-L.; Liao, T.-T.; Chen, Y.-W.; Chen, J.-D. Formation of entangled Co(II) coordination polymers based on bis-pyridyl-bis-amide and angular dicarboxylate ligands: A structural comparison. *CrystEngComm* **2023**, *25*, 5575–5587. [CrossRef]
24. Lu, X.-Q.; Zhang, L.; Chen, C.-L.; Su, C.-Y.; Kang, B.-S. Syntheses and 1D structures of organic–inorganic hybrid polymers combining $M(ClO_4)_2$ (M = Cd, Zn) junctions and the semi-flexible bis-pyridyl ligand 3-pmpmd (N,N′-bis(3-pyridylmethyl)pyromellitic diimide). *Inorg. Chim. Acta* **2005**, *358*, 1771–1776. [CrossRef]
25. Li, G.-B.; He, J.-R.; Pang, M.; Deng, H.-Y.; Liu, J.-M.; Su, C.-Y. Construction of 0D to 3D cadmium complexes from different pyridyl diimide ligands. *Dalton Trans.* **2012**, *41*, 4626. [CrossRef]
26. Li, G.-B.; Liu, J.-M.; Cai, Y.-P.; Su, C.-Y. Structural Diversity of a Series of Mn (II), Cd (II), and Co (II) Complexes with Pyridine Donor Diimide Ligands. *Cryst. Growth Des.* **2011**, *11*, 2763–2772. [CrossRef]
27. Chai, W.; Lu, X.; Bi, W.; Song, J.; Kang, B. Non-Parallel Stacking of a One-Dimensional Rod and Loop Chain Cd (II) Complex with the Semi-Rigid 3,3′-Bipyridyl Ligand. *J. Chem. Crystallogr.* **2010**, *40*, 740–745. [CrossRef]
28. Lu, X.-Q.; Jiang, J.-J.; Loye, H.-C.; Kang, B.-S.; Su, C.-Y. A Noninterpenetrated 1D Molecular Ladder and 2D Butterfly Network: Effect of Positional Isomerism of Semirigid Bis(pyridylmethyl)pyromellitic Diimide Ligands on the Architecture of Their Metal(II) Complexes. *Inorg. Chem.* **2005**, *44*, 1810–1817. [CrossRef]
29. Li, X.; Fan, X.; Zeng, Q. Supramolecular Coordination Polymers by Self-assembling of Bis-monodentate Ligands with HgI_2. *Int. J. Mol. Sci.* **2007**, *8*, 29–41. [CrossRef]
30. Yan, B.; Ma, R.; Chu, Z.; Ding, L.-Q.; Long, Y.-L.; Chen, L.-X.; Lu, Q.; Bao, F. 2D Cationic Metal-Organic Frameworks of Ag^+ with Mixed Ligands (Semi-Rigid Dipyridyl, 3-pmpmd, and Diphosphine, dppe). *J. Inorg. Organomet. Polym.* **2010**, *20*, 809–815. [CrossRef]
31. Yu, Z.-Q.; Pan, M.; Jiang, J.-J.; Liu, Z.-M.; Su, C.-Y. Anion Modulated Structural Diversification in the Assembly of Cd(II) Complexes Based on a Balance-like Dipodal Ligand. *Cryst. Growth Des.* **2012**, *12*, 2389–2396. [CrossRef]
32. Govindaraj, M.; Huang, W.-C.; Lee, C.-Y.; Lakshmanan, V.; Liu, Y.-H.; So, P.B.; Lin, C.-H.; Chen, J.-D. Structural Diversity of Mercury(II) Halide Complexes Containing Bis-pyridyl-bis-amide with Bulky and Angular Backbones: Ligand Effect and Metal Sensing. *Int. J. Mol. Sci.* **2022**, *23*, 7861. [CrossRef] [PubMed]
33. Blatov, V.A.; Shevchenko, A.P.; Proserpio, D.M. Applied topological analysis of crystal structures with the program package ToposPro. *Cryst. Growth Des.* **2014**, *14*, 3576–3586. [CrossRef]
34. Huang, X.-M.; Li, G.-B.; Pan, R.-K.; Liu, S.-G. Synthesis and crystal structure of two coordination polymers based on *N*,*N*′-bis(3-pyridylmethyl)pyromellitic diimide and fluorescence thiocyanate sensing. *Transit. Met. Chem.* **2020**, *45*, 187–193. [CrossRef]
35. Li, G.-B.; Huang, X.-M.; Pan, R.-K.; Liu, S.-G. Liu. Diverse 1D chains supramolecular structures of *N*,*N*′-bis(3-pyridylmethyl)pyromellitic diimide and fluorescence iodide sensing. *Spectrochim. Acta A Mol. Biomol. Spectrosc.* **2020**, *229*, 117941. [CrossRef]
36. Spek, A.L. checkCIF validation ALERTS: What they mean and how to respond. *Acta Cryst.* **2020**, *76*, 1–11. [CrossRef]
37. Korin, E.; Froumin, N.; Cohen, S. Surface Analysis of Nanocomplexes by X-ray Photoelectron Spectroscopy (XPS). *ACS Biomater. Sci. Eng.* **2017**, *3*, 882–889. [CrossRef]
38. Li, Z.-J.; Yue, Z.; Ju, Y.; Wu, X.; Ren, Y.; Wang, S.; Li, Y.; Zhang, Z.-H.; Guo, X.; Lin, J. Ultrastable Thorium Metal-Organic Frameworks for Efficient Iodine Adsorption. *Inorg. Chem.* **2020**, *59*, 4435–4442. [CrossRef] [PubMed]
39. Bruker AXS. *APEX2, V2008.6*; SAD ABS V2008/1, SAINT+ V7.60A, SHELXTL V6.14; Bruker AXS Inc.: Madison, WI, USA, 2008.
40. Sheldrick, G.M. A short history of SHELX. *Acta Cryst.* **2015**, *71*, 3–8.

Disclaimer/Publisher's Note: The statements, opinions and data contained in all publications are solely those of the individual author(s) and contributor(s) and not of MDPI and/or the editor(s). MDPI and/or the editor(s) disclaim responsibility for any injury to people or property resulting from any ideas, methods, instructions or products referred to in the content.